RESEARCH ARTICLE

Macromolecular Materials and Engineering
Open Access
www.mame-journal.de

Fabrication of Multifunctional Nanofiber Mats by Emulsion Electrospinning of TPU/Fish Skin Gelatin Incorporating Plant Extract-Based Therapeutic Oil for Wound Dressing Applications

*Rüya Keskinkaya, Arzu Yıldırım, Şeyma Çağlayan, Eray Sarper Erdoğan, Yurdanur Türker, Dilara Nur Dikmetaş, Funda Karbancıoğlu - Güler, Saime Batirel, Fatma Seniha Güner, and Melek Erol-Taygun**

In this study, for the first time thermoplastic polyurethane (TPU), fish skin gelatin (FSG), and *H. perforatum* oil (HPO) combine to form a new nanofiber material by using the emulsion electrospinning technique. Scanning electron microscope (SEM), Fourier transform infrared (FTIR) spectroscopy, and thermogravimetric analysis (TGA) are used for the characterization studies. Moreover, antibacterial activities, in vitro wound healing and cytotoxicity of the TPU mats are also investigated. The SEM investigations reveal that the average diameters of defect-free TPU nanofiber mats with diverse HPO concentrations are ≈400–500 nm and suitable to mimic the native extracellular matrix (ECM) with these values. Moreover, although there is no antibacterial activity in the control TPU mat, the addition of the tannic acid crosslinker and 12% of HPO to the nanofiber mat acquires a 31.3% inhibition against *Staphylococcus aureus* and a 21.0% against *Escherichia coli*. Furthermore, the TPU nanofiber mat with the highest HPO concentration (12%) is non-toxic to the cells and tends to promote healing in vitro assay. Overall results indicate that the wound healing properties of the obtained HPO-encapsulated TPU nanofiber mats can be a promising candidate for wound dressing applications.

1. Introduction

Wound dressings are biomedical products that can be produced from natural or synthetic materials. They provide a rapid and aesthetic recovery of the injured tissue and support the recovery of biological activities while reducing inflammation.

Nowadays, the production of wound dressing materials with different properties designed specifically for different wound types attracts significant attention. An ideal dressing should absorb the wound exudate and facilitate gas permeability for providing the ideal moisture balance in the wounded area. These dressing materials must be strong, highly elastic, stable, impermeable to bacteria, biocompatible, non-toxic, non-allergic, and easy to use. Moreover, they should be able to mimic the structure and function of the native extracellular matrix (ECM).[1–3]

Nanofiber production processes are extensively researched for simulating the

R. Keskinkaya
Program of Chemical Engineering
Istanbul Technical University
Graduate School
Istanbul 34469, Turkey

A. Yıldırım
Program of Polymer Science and Technology
Istanbul Technical University
Graduate School
Istanbul 34469, Turkey

The ORCID identification number(s) for the author(s) of this article can be found under https://doi.org/10.1002/mame.202500015

© 2025 The Author(s). Macromolecular Materials and Engineering published by Wiley-VCH GmbH. This is an open access article under the terms of the Creative Commons Attribution License, which permits use, distribution and reproduction in any medium, provided the original work is properly cited.

DOI: 10.1002/mame.202500015

Ş. Çağlayan
Faculty of Chemical and Metallurgical Engineering
Department of Bioengineering
Yıldız Technical University
Istanbul 34210, Turkey

E. S. Erdoğan, F. S. Güner, M. Erol-Taygun
Faculty of Chemical and Metallurgical Engineering
Department of Chemical Engineering
Istanbul Technical University
Istanbul 34469, Turkey
E-mail: erolm@itu.edu.tr

Y. Türker, F. S. Güner
Sabancı University Nanotechnology Research and Application Center (SUNUM)
Tuzla, Istanbul 34956, Turkey

D. N. Dikmetaş, F. Karbancıoğlu - Güler
Faculty of Chemical and Metallurgical Engineering
Department of Food Engineering
Istanbul Technical University
Istanbul 34469, Turkey

structure of ECM. There are several methods to fabricate the nanofiber structure. However, the electrospinning process is unique and noteworthy to conduct more research due to its distinctive properties and different production techniques.[4–11]

When attempting to electrospin two immiscible liquid phases, such as a dispersed oil phase inside a continuous water phase (O/W), emulsion electrospinning can be the preferred method. This technique generates the core-shell fibers and allows the designing of the mats to release the functional bioactive materials from the fiber scaffold over time, which possesses significance for the development of bioactive materials, wound dressing materials, and tissue engineering.[4,12,13] Besides mimicking the structure and function of the native ECM,[14,15] thanks to their porous structure, a higher specific surface area than the other nanofiber production methods, electrospun nanofibers also promote cell attachment[15] and cellular responses, transports the nutrient to the growing cells, and facilitates gas permeability through its excellent 3D irregular interconnections.[15,16]

In various studies in the literature, thermoplastic polyurethane (TPU) was used as a polymer matrix with different biopolymers and bioactive components to fabricate electrospun nanofiber mats for wound dressing applications.[1,2,14,15,17–21] TPU is a synthetic polymer known for its excellent mechanical strength, flexibility, and durability. These properties allow it to withstand the stress of daily activities, maintaining consistent protection at the wound site. Its mechanical and biological advantages in wound dressings are well-established.[22–24] The similarity between the carbamate groups in TPU and amide bonds in human proteins enhances biocompatibility[15,20] while this polymer also offers elasticity, processability, and high transparency. Additionally, TPU's impermeability to liquids and microorganisms help maintain a sterile environment and promote healing, making it an ideal material for biomedical research.[22]

Gelatin is a natural, biocompatible polymer that mimics the structure and function of the ECM,[3] which is a key component of connective tissues. As a different form of collagen, gelatin interacts favorably with biological tissues, promoting key processes for wound healing, including cellular adhesion, proliferation, and migration. Its biodegradability allows gradual absorption by the body without adverse reactions, making it a safe and effective material for medical applications.[25–27] Fish skin gelatin (FSG), in particular, is preferred over bovine and porcine gelatins due to its lower immunogenicity, high biocompatibility, biodegradability, sustainability, environmental benefits,[28] functional versatility, multi-functionality,[29–31] and its advantages in terms of cultural acceptance and religious neutrality.[32] Moreover, its hydrophilicity, low cost, water-retaining capacity, and ability to promote hemostasis and blood coagulation effect are suitable for a wound dressing material.[33,34] *H. perforatum* oil (HPO) is a plant extract, which is traditionally used in Türkiye as a home remedy for thermal burns, skin diseases, bruises, and cuts.[35] It is typically prepared by putting dried yellow-flowered *H. perforatum*, which is a medicinal plant, into the olive oil and exposing it to the sunlight for around four weeks until obtaining a dark red oil.[35,36] This plant contains hyperforin and hypericin, known for their antimicrobial properties.[37] HPO is particularly effective against Gram-positive bacteria than Gram-negative ones.[36,38] Furthermore, studies also confirmed the wound-healing activity of HPO in rat models and its ability to accelerate recovery after cesarean section in female patients.[36] HPO has emerged as an attractive to current bioactive components used in wound dressings, such as silver,[39] povidone-iodine (PVP-I)[40] and essential oils, due to its lower cost and fewer toxicity concerns. In this study, HPO, an endemic plant extract traditionally used for burn treatments in Turkey,[41] was selected for its abundance, affordability, and accessibility, as an innovative bioactive component for wound dressing development.

To assess the effectiveness of the nanofiber mats fabricated in this study, we considered the average diameters and morphologies of TPU electrospun fiber mats from literature, along with the presence of bioactive components with wound healing or antibacterial properties in the fiber mats (and their efficiencies), as the primary performance indicators. Although there is no optimal fiber diameter size that seems promising for fibroblast migration and ECM imitation and researchers continue to explore optimal designs for wound dressing application, the nanofibers diameters up to 500 nm are considered convenient to mimic the architecture of native ECM.[42,43] In recent studies, without incorporating any bacterial or healing-promoting component, even though obtained TPU electrospun fibers were at the sub-micrometer levels,[2,14,16,18,19] and these studies did not present any test results regarding antibacterial properties. On the other hand, TPU fibers functionalized with different bioactive agents and possess good antibacterial efficiency[15,17,20,21] showed larger fiber diameters around the scale of several micrometers, which would not be significantly effective in mimicking the native ECM. Only few studies have developed TPU-based nanofiber mats with bioactive components,[44–46] demonstrating promising results in effective wound healing, reduced fibrosis, inflammation, antibacterial protection,[45] and fast wound closure.[46] However, limited knowledge and achievements in this area highlights the need for further investigation to fully explore the potential of multifunctional bioactive components in TPU electrospun nanofibers. In this study, a new candidate as a wound dressing material in the nanofiber structure was engineered by using TPU, FSG, and HPO for the first time by the emulsion electrospinning technique. TPU, a medical-grade synthetic polymer, was chosen as the primary polymer matrix thanks to its mechanical strength and elasticity; FSG, a natural polymer, was included in the structure to increase cellular affinity; and HPO was used for its wound healing and antibacterial properties as a natural and cost-effective bioactive component to add functionality to nanofiber mats. The obtained HPO-encapsulated TPU/FSG nanofiber mats may be a promising candidate for wound dressing applications.

S. Batirel
School of Medicine
Department of Medical Biochemistry
Marmara University
Istanbul, Maltepe 34854, Turkey

 © 2025 The Author(s). Macromolecular Materials and Engineering published by Wiley-VCH GmbH

14392054, 2025, 10, Downloaded from https://onlinelibrary.wiley.com/doi/10.1002/mame.202500015 by Turkey Cochrane Evidence Aid, Wiley Online Library on [20/10/2026]. See the Terms and Conditions (https://onlinelibrary.wiley.com/terms-and-conditions) on Wiley Online Library for rules of use; OA articles are governed by the applicable Creative Commons License

2. Experimental Section

2.1. Materials

Medical-grade TPU, Tecoflex EG-80A (Mw = 110.000), was procured from Lubrizol (Spain). Gelatin (G7041), derived from cold-water fish skin, was purchased from Sigma-Aldrich (USA). HPO was sourced from a local supplier in Türkiye. Glacial acetic acid and Tannic acid (China) were both obtained from Sigma-Aldrich. Nonionic surfactants Triton X and Tween 80 were supplied by Merck (Germany and France, respectively).

2.2. Preparation Procedure of TPU/FSG/HPO Emulsion

The hydrophobic components were made ready in phase A, while the hydrophilic components were in phase B.

Phase A: TPU was dissolved in glacial acetic acid by stirring at 80 °C for 2 h. Then, HPO was added at different percentages (wt) of the total polymer weight for each sample and mixing of phase A was continued.

Phase B: FSG was slowly added to a solution mixture containing 1 mL of glacial acetic acid and 0.5 mL of deionized water. The mixture was stirred at 50 °C until completely dissolved. Then, Tween 80 (T-80) was added, and the stirring process continued for 2 h at 37 °C. Afterward, to crosslink the gelatin, 15% (wt.) of tannic acid (TA) was prepared by dissolving the TA into a different glass vial in a 1:1(v/v) glacial acetic acid and deionized water co-solvent. Then, the tannic acid solution was added to the gelatin solution drop by drop while gently stirring, and stirring was continued for 3 h.

The mixing of phase A and phase B: The phase B was added to phase A drop by drop under gentle mixing and stirring continued for 2 h. In a separate glass vial, a 1% Triton-X solution was prepared in deionized water and added to the emulsion to enhance the stability. Then, the emulsion was stirred at room temperature for 48 h until the electrospinning process began.

Emulsion electrospinning: A laboratory-scale electrospinning unit (INNOVENSO Innovative Engineering Solutions) was used in this study. The prepared emulsion was loaded in a 5 mL plastic syringe, attached to an 18-gauge blunt-end needle, and then replaced into an injection pumping unit. Meanwhile, the metal collector plate was covered with aluminum to collect nanofibers. The process conditions of electrospinning were 20 kV of applied voltage, 20 cm of tip-to-collector distance (TCD), and a flow rate of 0.5 mL h^{-1}.

Preparation of the samples: Following the method described above, TPU nanofiber mats with different concentrations of HPO were prepared, namely E-1 (5%), E-2 (8%), E-3 (10%), and E-4 (12%). A schematic representation of sample preparation was given in **Figure 1**. To demonstrate the impact of including HPO on the properties of TPU nanofiber scaffolds, two control samples were also fabricated without HPO. Control sample C-1 did not contain HPO but included tannic acid as a crosslinker, while control sample C-2 was prepared without both tannic acid and HPO. The compositions of the emulsions for electrospinning were given in **Table 1**. Furthermore, images of prepared emulsions and their electrospun mats were presented in Appendix, Figure A1.

Table 1. The Compositions of Prepared TPU/FSG/HPO emulsion.

Sample codes	The composition ratios of the emulsions
C-1	**Control-1** (no HPO, crosslinked with tannic acid)
	A phase: 9% TPU + 5% HPO
	B phase: 1% FSG + 0.2% T-80 + 0.15% TA
	No HPO & crosslinked with TA
C-2	**Control-2** (no HPO, no tannic acid)
	A phase: 9% TPU + 5% HPO
	B phase: 1% FSG + 0.2% T-80 + 0.15% TA
	No HPO & No TA
E-1	**Emulsion-1: 5% HPO** Containing
	A phase: 9% TPU + 5% HPO
	B phase: 1% FSG + 0.2% T-80 + 0.15% TA
	5 (wt.) % HPO & crosslinked with TA
E-2	**Emulsion-2: 8% HPO** Containing
	A phase: 9% TPU + 8% HPO
	B phase: 1% FSG + 0.2% T-80 + 0.15% TA
	8 (wt.) % HPO & crosslinked with TA
E-3	**Emulsion-3: 10% HPO** Containing
	A phase: 9% TPU + 10% HPO
	B phase: 1% FSG + 0.2% T-80 + 0.15% TA
	10 (wt.) % HPO & crosslinked with TA
E-4	**Emulsion-4: 12% HPO** Containing
	A phase: 9% TPU + 12% HPO
	B phase: 1% FSG + 0.2% T-80 + 0.15% TA
	12 (wt.) % HPO & crosslinked with TA

2.3. Characterization of the Obtained Samples

2.3.1. Scanning Electron Microscopy Analysis

Scanning Electron Microscope (SEM, JEOL, JSM-6010LV) was used to examine the morphologies of the nanofibers. Nanofiber mats were placed on a coverslip and sputter-coated within Cressington Sputter Coater 108auto by thin Au/Pd under 40 mA for 40 s (3 times). The images of the samples were taken. Afterward, 50 random nanofiber diameters were measured for each sample by the Image J program.

2.3.2. Fourier Transform Infrared Spectroscopy

To enlighten the chemical structure of the HPO incorporated TPU nanofiber samples, the characterization was conducted by the Fourier transform infrared spectroscopy (FTIR) technique at a NICOLET 6700, Thermo Scientific brand device in ATR mode. All data were recorded by means of a diamond internal reflective element in the range of 600–4 000 cm^{-1} and normalized.

2.3.3. Thermogravimetric Analysis

Thermogravimetric analysis (TGA) of the samples was performed by a thermal analyzer (Perkin Elmer SII Diamond) in a nitrogen atmosphere by heating from 25 to 550 °C at the rate

© 2025 The Author(s). Macromolecular Materials and Engineering published by Wiley-VCH GmbH

14392054, 2025, 10, Downloaded from https://onlinelibrary.wiley.com/doi/10.1002/mame.202500015 by Turkey Cochrane Evidence Aid, Wiley Online Library on [20/10/2026]. See the Terms and Conditions (https://onlinelibrary.wiley.com/terms-and-conditions) on Wiley Online Library for rules of use; OA articles are governed by the applicable Creative Commons License

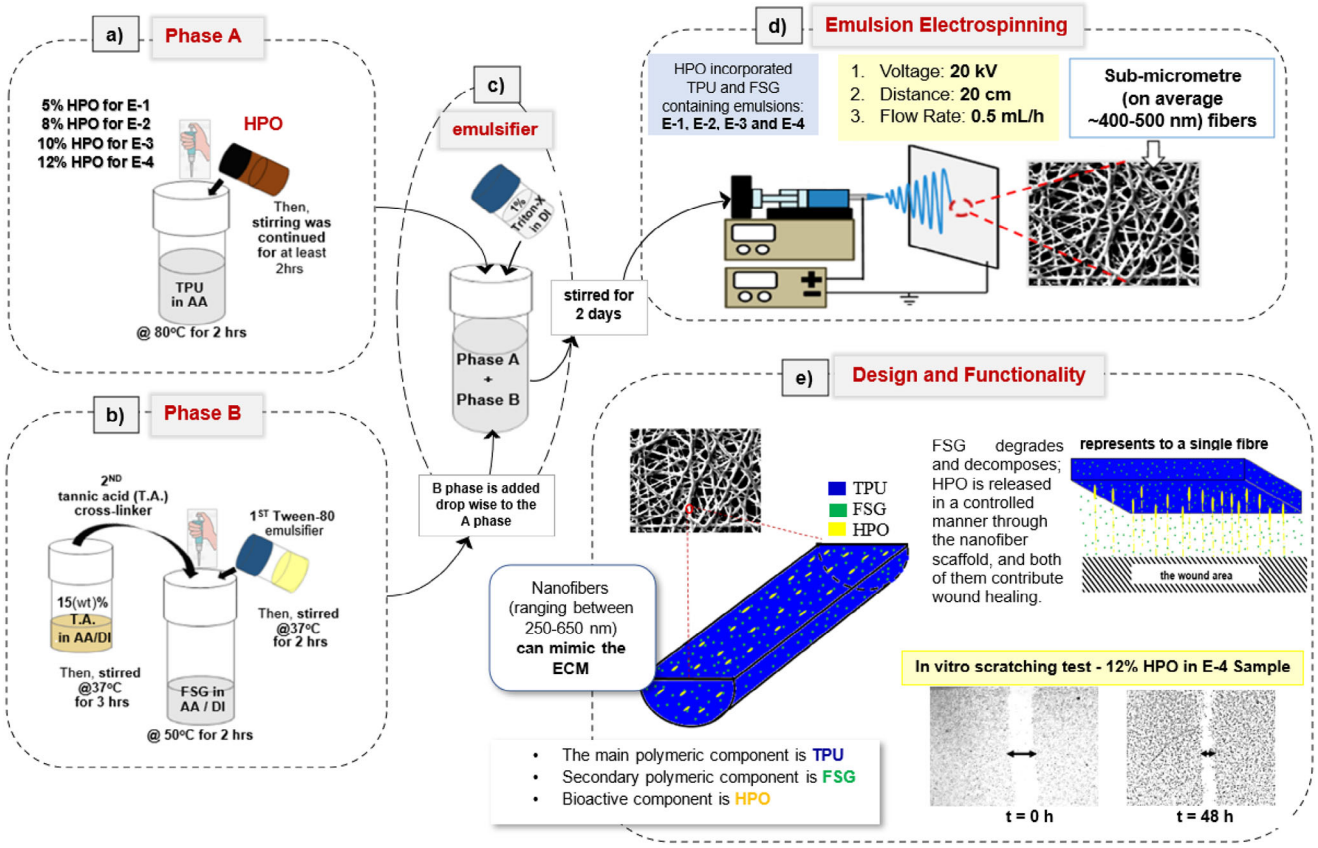


Figure 1. Schematic summary of a) the preparation of Phase A (TPU phase); b) Phase B (gelatin phase); c) emulsions (E-1, E-2, E-3, E-4); d) the emulsion electrospinning process; and e) the design, explanation, and functionality of HPO-encapsulated TPU–gelatin nanofiber mats are highlighted, demonstrating their healing efficacy through in vitro scratch tests.

of 5 °C min^{-1}. Before analysis, gelatin containing samples were kept in an oven at 37 °C and dried for one day.

2.3.4. Water Contact Angle

The water contact angle (WCA) measurement was performed using the Biolin Scientific Theta Lite optical tensiometer. Each sample was electrospun for 3 h under the same process conditions, cut in sizes of 20 mm × 50 mm without stripping from the aluminum foil and fixed on both ends with tape on the stage to prevent disruption of their shape. 5 µL of distilled water was passed from the syringe to the mat surface, and contact angles were measured. For each sample, five measurements were recorded.

2.3.5. Water Vapor Transmission Rate (WVTR)

The WVTR of the electrospun mats was detected by the ASTM E96-00 standard.[2,47] They were cut using a round mold of 2.01 cm^2 and taped with sticky aluminum foil. The prepared sample was bonded to completely cover the mouth of glass vials filled with silica. The sample, along with the glass vials, was weighed and recorded as W_1. It was then placed in a desiccator containing a saturated solution of NaCl salt. The WVTR of the sample was calculated at specific time intervals (W_2) using the Equation (1) and expressed in the unit of g m^{-2} day^{-1}.

$$\mathrm{WVTR}\left(\mathrm{g\ m^{-2}\ day^{-1}}\right) = \frac{W_2 - W_1}{W_1.A.\Delta t} \quad (1)$$

where W_1: initial mass of the glass bottle (g), W_2: final mass of the glass bottle (g), A: exposed area (m^2), ΔT: exposure time (day).

For each mat, 3 test samples were prepared, and the water vapor permeability rates were calculated over the average values.

2.3.6. Fluid Handling Capacity

The fluid handling capacity (in other words, water absorbency) of the samples was carried out according to the BS EN 13726-1:2002 standard test method.[47–49] First, a salt solution of ionic composition equiv. to human serum or wound exudate was prepared by weighing 0.368 g $CaCl_2$ and 2.298 g NaCl, mixing in 1 L deionized water using a magnetic stirrer and heating to 37 °C. The solution

© 2025 The Author(s). Macromolecular Materials and Engineering published by Wiley-VCH GmbH

14392054, 2025, 10, Downloaded from https://onlinelibrary.wiley.com/doi/10.1002/mame.202500015 by Turkey Cochrane Evidence Aid, Wiley Online Library on [20/10/2026]. See the Terms and Conditions (https://onlinelibrary.wiley.com/terms-and-conditions) on Wiley Online Library for rules of use; OA articles are governed by the applicable Creative Commons License

was incubated in a laboratory oven at 37 ± 1 °C. Each sample was electrospun under the same process conditions for 3 h, cut in 5 cm × 5 cm dimensions, peeled off the aluminum foil, placed in Petri dishes and weighed (W_1). Afterward, salt solution was dispensed into the Petri discs, in amounts corresponding to 40 times the weight of each sample (at a ratio of 1:40 (wt./v)). These Petri discs were incubated at 37 °C for 30 min. At the end of this conditioning, the samples were taken from the laboratory oven and suspended from one corner for 30 s with the help of tweezers, and after dripping off the excess water, they were weighed (W_2). Then, fluid handling capacity was calculated according to Equation (2).

$$\text{Fluid handling capacity} = \frac{W_2 - W_1}{W_1} \quad (2)$$

where W_1 is the mass of specimens before testing, W_2, the solution absorbed mass of specimens after testing.

2.3.7. pH Change of the External Solution in the Presence of Nanofiber Mats

For each 5 mg sample that was weighed into a beaker, 500 mL of deionized water was added and left to be stirred at room temperature with a magnetic stirrer at the same speed. So, the samples were suspended in deionized water at a ratio of 1:100 (w/v). After calibrating the device at pH 4, 7, and 10, pH was measured using a pH meter combined with a pH electrode (Mettler Toledo Benchtop pH meter). The pH values of the wound dressings were recorded by measuring first after 3 h and then 24 h later.

2.3.8. Antibacterial Activity Test

The antibacterial efficiency of samples was evaluated quantitatively by the optical density (OD) technique against Escherichia coli ATCC 25922 and Staphylococcus aureus ATCC 25923 according to the procedure described by Akturk.[50] Bacterial cultures were grown and incubated individually at 37 °C for 24 h in 100 mL of nutrient broth (NB), (1 g L^{-1} meat extract, 5 g L^{-1} peptone from meat, 2 g L^{-1} yeast extract, 5 g L^{-1} NaCl). Following incubation, a bacterial suspension was prepared at 10^4 CFU/mL concentration, and 10 µL of it was dispersed into the 10 mL fresh NB solution. Approximately 50 mg of the nanofiber mats were weighed and irradiated by ultraviolet light for 30 min on each side. Then, nanofiber mats were placed into bacteria inoculated test tubes and incubated at 37 °C for 24 h on a rotary shaker. The inoculated NB without control samples was used as the positive control. After incubation, the absorbance of the NB at 600 nm (OD600) was measured by a UV–vis spectrophotometer (Biotek, Synergy HT). The bacterial reduction (%) was calculated with Equation (3), in which the term "Abs control" indicates the absorbance of the inoculated NB without nanofiber mat and the term "Abs sample" is the absorbance of the inoculated NB with nanofiber mat.

$$\text{Bacterial reduction (\%)} = \frac{Abs\ control - Abs\ sample}{Abs\ control} \times 100 \quad (3)$$

2.3.9. In Vitro Wound Healing Assay

To determine the wound-healing features of the samples, a wound-healing assay using fibroblast cells was performed. Human dermal fibroblast cells (American Tissue Culture Collection, Manassas, VA, USA), PCS-201-012, were seeded into collagen-coated 24-well tissue culture plates which were maintained at 37 °C and 5% CO_2 conditions. After the attachment of cells, a scratch was made with a pipette tip within the monolayer of the cells. The cells were treated with E-4 sample (a TPU nanofiber mat containing 12% HPO) in growth medium for 48 h. Photomicrographs of the scratched area were taken by a microscope (Carl Zeiss, Jena, Germany) at the beginning of the incubation and after 48 h incubation period without changing the cell culture medium. The wound width at 0 h and 48 h was measured, and the ratio of wound width at 0 h to that at 48 h was calculated. Statistical analysis was performed using a student's *t*-test with a significance level set at $p \leq 0.05$. The test was performed at least in duplicate and in two independent experiments.

3. Results and Discussions

3.1. Scanning Electron Microscopy Analysis

Since TPU is the dominant component of the obtained samples, the average diameters and morphologies of recent studies on TPU electrospun fiber production were evaluated altogether with whether or not any bioactive component, possessing wound healing or antibacterial properties, was included in the fiber scaffolds. According to recent studies, the average diameters of the fabricated TPU electrospun fibers without any antibacterial or healing-promoting components were 225 ± 25 nm,[2] 558 ± 18 nm,[14] 100.6 ± 17.831 nm,[19] and 117.31 ± 12.6 nm[16] at the sub-micrometer levels. In contrast, the TPU fibers functionalized with different antibacterial agents[15,17,20,21] showed larger fiber diameters around a few micrometers scale. On the other hand, in this study, as seen from **Figure 2**, SEM images of fabricated TPU mats indicated the generation of homogeneous, bead-free nanofibers even after the inclusion of HPO. The average diameters of fabricated TPU nanofiber mats containing HPO at varying concentrations like E-1 (5%), E-2 (8%), E-3 (10%), and E-4 (12%) were measured as 410 ± 158 nm, 424 ± 157 nm, 466 ± 192 nm, and 514 ± 136 nm, respectively. While the HPO concentration increased from 5% to 12%, the TPU nanofiber mats maintained almost the same diameters in terms of standard deviations. The ideal wound dressing candidate material must have an average fiber diameter around the sub-micrometer level. Producing sub-micrometric fibers increases the capillary gap, forms more porosity in scaffolds, helps to release the vapor from the wound environment, and mimics the structure of native ECM.[42,43,51] In the literature, Chong and colleagues created a layered wound dressing by direct electrospinning of a blend of poly(ϵ-caprolactone) (PCL) and gelatin with an average fiber diameter of 470 ± 120 nm onto a commercial acrylic polyurethane dressing.[52] Unnithan et al. developed electrospun composite nanofiber mats using polyurethane–cellulose acetate–zein with an average fiber diameter ranging from 400 to 700 nm.[53] Furthermore, Wang and coworkers developed a composite nanofibrous mat by combining

© 2025 The Author(s). Macromolecular Materials and Engineering published by Wiley-VCH GmbH

14392054, 2025, 10, Downloaded from https://onlinelibrary.wiley.com/doi/10.1002/mame.202500015 by Turkey Cochrane Evidence Aid, Wiley Online Library on [20/10/2026]. See the Terms and Conditions (https://onlinelibrary.wiley.com/terms-and-conditions) on Wiley Online Library for rules of use; OA articles are governed by the applicable Creative Commons License

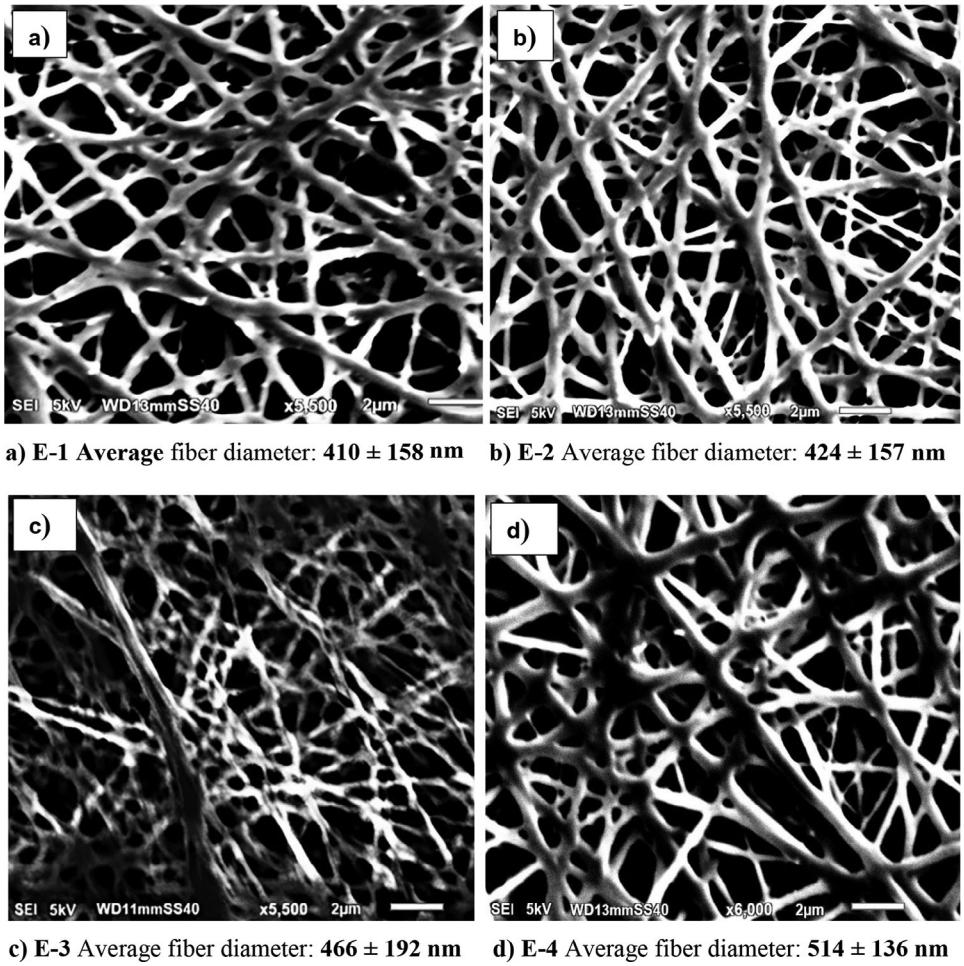


Figure 2. The Scanning Electron Microscope Images of HPO Incorporated TPU Nanofiber Samples a) E-1, b) E-2, c) E-3, and d) E-4.

polyurethane, keratin, and silver nanoparticles for wound dressing, with an average fiber diameter of 622 ± 211 nm.[54] These nanofiber mats at the specified diameters enhanced cell adhesion, growth, proliferation, and accelerated wound healing.[52–54] Moreover, they achieved close biomimicry of the ECM.[52] Therefore, in this study, obtained TPU nanofiber mats imitate the native ECM structure with the fibers at sub-micrometer levels and provide microbial control, reducing inflammation with HPO possessing antibacterial and wound healing properties. SEM observations indicated that bioactive HPO-encapsulated TPU fiber scaffolds resulted in non-filmy and homogeneous bead-free images at nanometric scales.

3.2. Fourier Transform Infrared Spectroscopy

The FTIR spectra of TPU and FSG polymers, the HPO bioactive component, and C-1 and E-4 electrospun nanofibers were shown in **Figure** 3A. As the carbamate group (–NH–CO_2–) of the TPU macromolecule had functional groups similar to the amine bonds (–NH–CO–) within the gelatin, they both exhibited many mutual peaks.[2] Based on the figure, absorbance peaks in the E-4 and C-1 samples showed that characteristic absorbances of the TPU and FSG overlapped and became stronger than neat TPU. The peak at 3 302 cm^{-1} in TPU[55–57] due to the N-H stretching groups overlapping with the broad peak of FSG at 3 278 cm^{-1},[58–60] possibly related to the stretching vibrations of N-H or O-H groups, and shifted to a higher wavenumber of 3 322 cm^{-1} in C-1 control sample and 3 323 cm^{-1} in E-4 sample. Similarly, in TPU, the absorbance peaks corresponding to CH_2 stretching were observed at 2 921, 2 851, and 2 797 cm^{-1}.[55,57] These peaks overlapped with the C-H stretching vibrations of proteins in FSG, which appear at 2 941 and 2 881 cm^{-1}.[58] In the C-1 control sample, these CH_2 peaks were detected at 2 939, 2 856, and 2 800 cm^{-1}; while in the E-4 sample, they appeared at 2 927, 2 854, and 2 799 cm^{-1}.

Furthermore, in both C-1 and E-4 samples, the characteristic peaks of TPU in the amide-I, amide-II, and amide-III regions coincided with the absorbance peaks of FSG. In the amide-I region, the stretching of the free (C═O) groups at 1 717 cm^{-1} and H-bonded C-O at 1 698 cm^{-1} in TPU coincided with the C-O stretching functional groups of FSG at 1 633 cm^{-1}[57,59,60] and emerged at 1 716 and 1 694 cm^{-1} in C-1, and 1 717 and 1 694 cm^{-1} in E-4. Likewise, in the amide-II region, the peak indicating N-H bend-

 © 2025 The Author(s). Macromolecular Materials and Engineering published by Wiley-VCH GmbH

14392054, 2025, 10, Downloaded from https://onlinelibrary.wiley.com/doi/10.1002/mame.202500015 by Turkey Cochrane Evidence Aid, Wiley Online Library on [20/10/2026]. See the Terms and Conditions (https://onlinelibrary.wiley.com/terms-and-conditions) on Wiley Online Library for rules of use; OA articles are governed by the applicable Creative Commons License

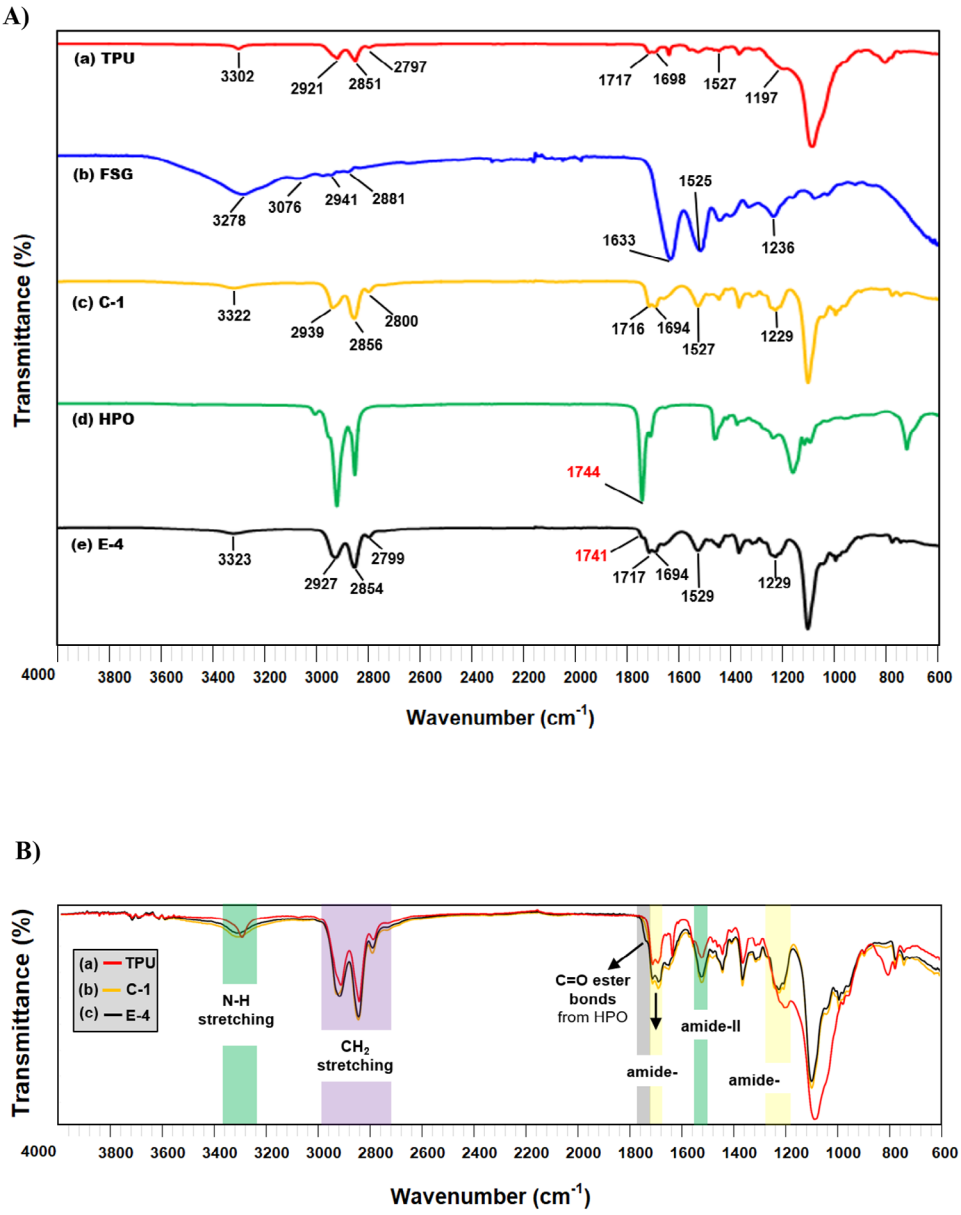


Figure 3. FTIR spectra of polymers and electrospun nanofibers.

ing and C-N stretching at 1 527 cm^{-1} wavenumber in the urethane structure[57] matched up with the absorbance peak seen at 1 525 cm^{-1}[58] in FSG, and it became visible at 1 527 cm^{-1} wavenumber in C-1 control sample and 1 529 cm^{-1} wavenumber in E-4 sample. Last, in the amide-III region, the absorbance peak of TPU at 1 197 cm^{-1} (C-N stretching)[57] coincided with the FSG at 1 236 cm^{-1}[58] and was detected at 1 229 cm^{-1} both in C-1 and E-4 samples. Overall, the FTIR results confirmed that the successful incorporation of TPU and FSG into the C-1 control and E-4 samples, with no significant alterations to their chemical structures, and molecular interactions between TPU and FSG polymers were demonstrated.

On the other hand, to show the successful incorporation of HPO into TPU nanofiber mats, the FTIR spectra of the C-1 sample were compared with E-4. As shown in **Figure** 3A, the most distinctive absorbance peak of HPO seen at 1 744 cm^{-1} wavelength was attributed to the stretching of carbonyl (C=O) groups present in the ester bonds of the oil. Following that, in Figure 3B, comparing the FTIR spectra of the control sample C-1 (yellow line) with the oil-containing dressing mat E-4 (black line), the absorbance peak observed only in E-4 unlike C-1 at 1 741 cm^{-1} indicated the successful incorporation of HPO into the E-4 nanofibers.

3.3. Thermogravimetric Analysis

The thermal properties of samples were investigated by TGA, which is an effective tool to show the properties of the sample's thermal decomposition temperature, thermal stability and the amount of moisture absorbed in them.[60–62] The mass loss

© 2025 The Author(s). Macromolecular Materials and Engineering published by Wiley-VCH GmbH

14392054, 2025, 10, Downloaded from https://onlinelibrary.wiley.com/doi/10.1002/mame.202500015 by Turkey Cochrane Evidence Aid, Wiley Online Library on [20/10/2026]. See the Terms and Conditions (https://onlinelibrary.wiley.com/terms-and-conditions) on Wiley Online Library for rules of use; OA articles are governed by the applicable Creative Commons License

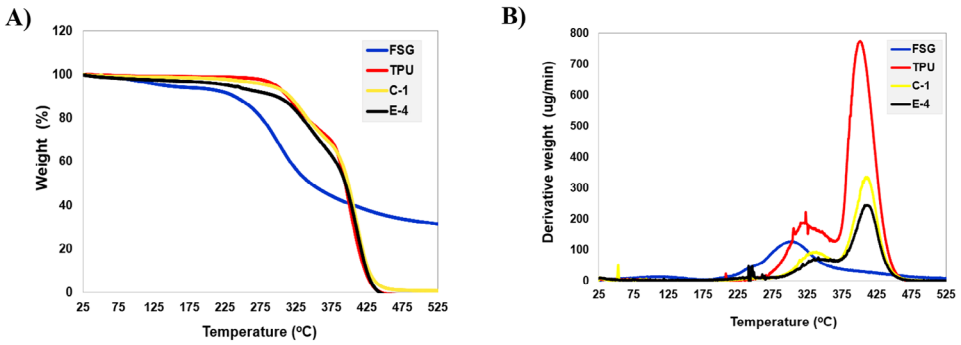


Figure 4. TGA curves; a) weight (%), and b) derivative weight.

rates illustrated the distinct degradation patterns of the composite nanofibers compared to TPU and FSG, suggesting successful incorporation of the components.

As seen in **Figure 4**, the thermal degradation of TPU, which was shown with the red curve, in the first decomposition phase started at 250 °C and peaks around ≈325 °C; in the second stage, around 400 °C, the mass loss rate of TPU reached around 50 (wt)%.[62,63] The mass loss curves of FSG demonstrated the two consecutive weight loss stages, as seen by the blue curves. The initial mass loss around the 70–150 °C range was attributed to the removal of physically adsorbed water molecules. As it can be seen from the second mass loss step of FSG, the mass loss is in the range from 150 to 260 °C, especially around 190–260 °C. This can be associated with the removal of chemisorbed water molecules and the degradation of gelatin polymer chains.[64–66]

While the weight loss (%) of the pure FSG sample at 260 °C was 14.6%, the mass loss of the C-1 control sample, which has a composite nanofiber mat containing FSG, reduced to 3.6% at the same temperature. The increase in heat resistance of the C-1 composite nanofiber compared to pure FSG is attributed to blending the gelatin with a synthetic polymer with higher thermal stability, such as TPU. In addition, the crosslinking FSG with tannic acid inside the C-1 composite mat also promotes thermal stability.[60,64,66]

The mass loss trends of the TG-DTG analysis of these samples, where the main component in the structure of both C-1 and E-4 samples is TPU, are similar to TPU. However, since the E-4 sample contains HPO in its structure, unlike the C-1 control sample, it was observed that HPO dispersed in the nanofiber mats decreased the thermal stability of the E-4 sample compared to C-1. Similarly, A. Pakolpakçıl et al. reported that the thermal stability of PLA nanofiber blended with HPO decreased compared to neat PLA.[61]

3.4. Water Contact Angle Measurements

The contact angle of the water droplets on the material surface is a good measurement of surface wettability. A contact angle of less than 90° indicates that it can wet the surface due to the hydrophilicity. If the contact angle is less than 10°, the surface feature can be defined as strongly super hydrophilic. Surfaces with WCA higher than 90° are characterized as non-wetting (hydrophobic) surfaces, while surfaces higher than 150° are called superhydrophobic.[67,68] The wound dressing materials should not be excessively hydrophilic or hydrophobic, which is suitable for patient comfort to support wound healing. Because, extremely hydrophilic dressings can cause severe damage to the healing area when removed due to the high cell adhesion and cell proliferation on the dressing surface. On the other hand, excessively hydrophobic dressings irritate the wound site.

The surface wettability of wound dressing materials is crucial for enhancing the bioactivity of the dressing as it affects the capacity for protein adsorption.[67–70] The interaction between proteins and dressing materials is primarily influenced by surface hydrophobicity. From a thermodynamic and chemical reaction standpoint, the main driving force for protein adsorption is the reduction of Gibbs adsorption-free energy (ΔG).[71,72] When the surface of wound dressing is hydrophobic, both the hydrophobic portions of the dressing material and the hydrophobic part of the protein surface cannot bond to the water molecule, triggering the release of the water molecules. Entropy increases and ends up with a decrease in Gibb's adsorption energy ($\Delta G = \Delta H - T\Delta S < 0$). In this way, the hydrophobic dressing surfaces facilitate the unfolding and spreading of the proteins and promote protein adsorption. Unlike hydrophobic surfaces, hydrophilic wound dressing surfaces form weak interactions and are not effective in binding protein.[69] Even though hydrophobic surfaces are generally known to bind proteins strongly and irreversibly to the surface, excessively hydrophobic dressing surfaces are not suitable for wound dressing applications due to causing denaturation of the proteins, which prevents their natural functions and irritates the skin.[73]

In most applications, wound dressings are produced by combining at least one hydrophobic as the upper layer (to keep the moisture in the wound area) with a hydrophilic phase (that interacts with the wound itself to absorb the wound exudate, and facilitates the hydrophilic polymer degradation).[68] In this study, components having various hydrophobic-hydrophilic properties (like TPU, FSG, and HPO) were used in a single phase to form an oil/water emulsion-based dressing material.

Accordingly, the mean WCA values of the prepared samples oil-free C-1 control samples and different ratios of HPO containing nanofiber samples, like E-1, E-2, E-3 & E-4, were shown in **Figure 5**. While the mean contact angle value of the C-1 sample was in the range of 83.2 ± 2.9°, contact angles of HPO contain-

© 2025 The Author(s). Macromolecular Materials and Engineering published by Wiley-VCH GmbH

14392054, 2025, 10, Downloaded from https://onlinelibrary.wiley.com/doi/10.1002/mame.202500015 by Turkey Cochrane Evidence Aid, Wiley Online Library on [20/10/2026]. See the Terms and Conditions (https://onlinelibrary.wiley.com/terms-and-conditions) on Wiley Online Library for rules of use; OA articles are governed by the applicable Creative Commons License

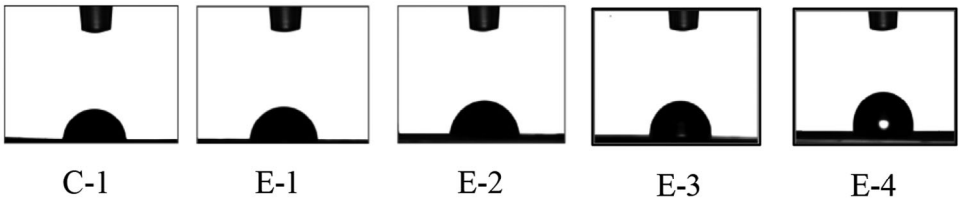


Figure 5. The WCA images of the control sample (C-1) and HPO containing samples like E-1, E-2, E-3, and E-4, respectively.

ing samples (the percentage of HPO samples was indicated in parentheses following the sample code): E-1(5%), E-2(8%), E-3(10%), and E-4(12%) were measured as 86.5 ± 3.0°, 94.3 ± 4.0, 100.4 ± 4.78°, and 100.7 ± 7.0°, respectively. The hydrophobicity of oil-containing samples is almost comparable at different concentrations when the standard deviations are taken into account.

It was seen that the sample surface becomes more hydrophobic with HPO incorporation and increased concentration. So, HPO incorporation is estimated to promote wound healing by reducing the protein adsorption Gibbs energy and improving protein adsorption to the dressing surface because of its hydrophobicity.[70,73] Furthermore, the prepared samples can be suitable wound dressing materials for patient comfort as not being excessively hydrophobic.

3.5. WVTR and Fluid Handling Capacity

For optimal wound healing, the ideal wound dressing should maintain a recommended water vapor loss rate of 2 000–2 500 g m^{-2} day^{-1}. If the rate is too high, the wound may dry out too quickly, causing the formation of scars. Conversely, if the rate is too low, it may lead to the accumulation of exudate in the wounded area, which can slow down the healing due to bacterial growth and infection. Therefore, it is crucial to ensure that wound dressings are designed to prevent wound dehydration while providing an optimal humidity ratio, promoting the best possible outcomes for patients.[14,51,74–77]

WVTRs of HPO containing TPU nanofiber mats E-2, E-3, and E-4 were measured as 1 789 ± 117, 1 991 ± 345, and 1 883 ± 140 g m^{-2} day^{-1} on average over the first three days, respectively. Then, as shown in **Figure 6**, the WVTRs of the mats decreased each day compared to the previous day. In the beginning, these mats exhibited close WVTR performance of the electrospun nanofiber mat developed by Mistry et al.,[2] including a blend of starch and TPU polymers, which possess an optimal WVTR of 1 956 ± 16.8 g m^{-2} day^{-1}. At the end of the 7 days, WVTRs of the same fabricated mats in this study reached 1 258 ± 74, 1 213 ± 292, and 992 ± 145 g m^{-2} day^{-1}, respectively. Since the inflammation phase and the amount of exudate in the wound

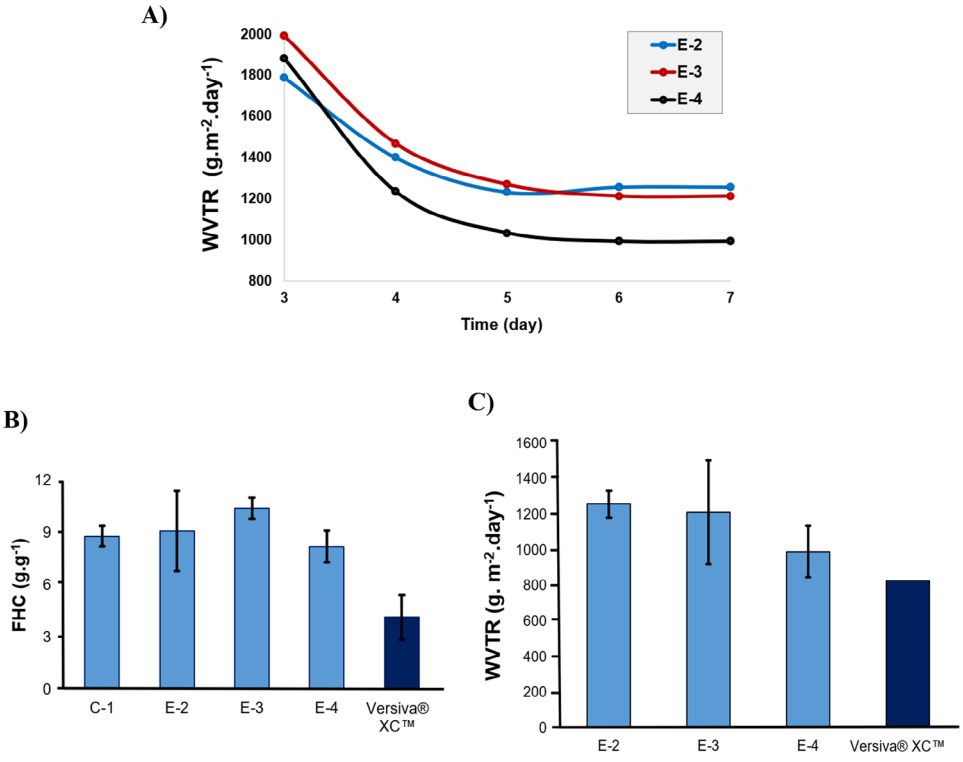


Figure 6. a) WVTR trends of fabricated mats. b) Fluid handling capacity (FHC) and c) WVTR.[48,78,79]

© 2025 The Author(s). Macromolecular Materials and Engineering published by Wiley-VCH GmbH

14392054, 2025, 10, Downloaded from https://onlinelibrary.wiley.com/doi/10.1002/mame.202500015 by Turkey Cochrane Evidence Aid, Wiley Online Library on [20/10/2026]. See the Terms and Conditions (https://onlinelibrary.wiley.com/terms-and-conditions) on Wiley Online Library for rules of use; OA articles are governed by the applicable Creative Commons License

area are likely to decrease at the end of the 4th day in the wound-healing process, the slowing pace of water vapor permeation over time can promote wound healing by preventing excessive dehydration in the wounded area. In addition, regarding the standard deviations, TPU nanofiber mats with various oil concentrations exhibited comparable water permeabilities when they reached stability.

Selecting a dressing with a high WVTR and absorbency is advantageous for treating highly exuding deep wounds. On the other hand, a slower WVTR and a lower absorbency capability will be more suitable in low-exuding superficial wounds. Considering this, the moisture-controlling performance of fabricated nanofiber mats was assessed by comparing their fluid handling capacities (FHCs) and WVTRs to the data of some commercial wound dressings like Kaltostat and Versiva XC, which were compiled from the literature.[48,78,79] According to the obtained literature data, the WVTR of alginate-based Kaltostat (2 434 ± 70.71 g m^{-2} day^{-1}) was approximately twice that of fabricated TPU mats. The lower WVTRs can be explained by the largest portion of the nanofiber mats comprised of TPU, a synthetic polymer with low absorbency properties. Additionally, the incorporation of HPO into TPU nanofiber samples was envisaged to be responsible for further decreasing the WVTR through increasing hydrophobicity. On the other hand, the WVTR of Versiva XC (830 g m^{-2} day^{-1})[48,78,79] (as shown in Figure 6C), and other commercial dressings like Tegaderm and Opsite,[76] which are recommended for controlling the moderately exudative wounds, were slightly lower than the obtained TPU nanofiber mats. In other words, WVTR values of the fabricated nanofibers slightly outperformed the Versiva XC dressing.

Besides WVTR, choosing a wound dressing material capable of absorbing the required amount of wound exudate for a specific wound type is also substantial. As shown in Figure 6B, fluid handling capabilities (FHCs) of the obtained HPO-containing samples E-2, E-3, and E-4 were calculated as 9.1 ± 2.3 g g^{-1}, 10.4 ± 0.6 g g^{-1} and 8.2 ± 0.9 g g^{-1}, respectively. When comparing the FHC of the fabricated TPU mats in this study with commercial dressings, the obtained TPU mats showed nearly half of the absorbency of Kaltostat (which is used for highly exuding wounds and has an absorbency of 18.44 ± 1.3 g g^{-1} according to the literature). Conversely, as shown in Figure 6B, the absorption capacity of the TPU nanofiber mats significantly exceeded that of the Versiva XC dressing, which has a reported absorbency of 4.16 ± 0.4 g g^{-1} according to the literature. This suggests that the TPU nanofiber mats possessed approximately double the absorbency of the Versiva dressing.[80,81]

The newly fabricated TPU nanofiber mats were expected to exhibit moisture control performance similar to that of Versiva XC, as shown in Figure 6B,C, considering their comparable WVTR and superior fluid handling capacity (FHC). While Versiva XC demonstrates good moisture management, its FHC is lower than that of the TPU mats, making the latter a promising dressing option for moderate to high exuding wounds.

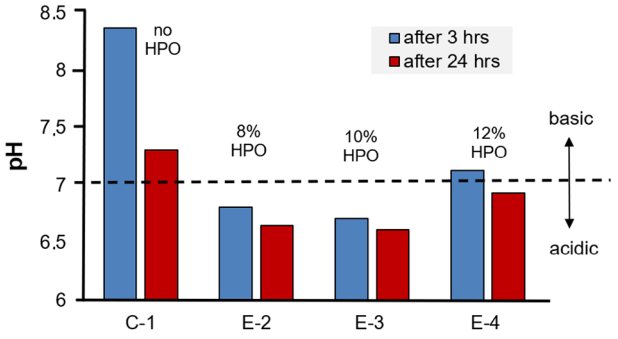


Figure 7. The solution-immersed pH values of C-1, E-2, E-3, and E-4 samples.

3.6. pH Change of the External Solution in the Presence of Dressings

The pH of a wound is critical for the healing process. Normally, the skin has a natural pH of 4.5–5.5. However, if the integrity of the skin is disrupted, the pH level increases since the slightly alkaline pH of the inner body parts reaches out to the skin surface. This change promotes the growth of harmful pathogens and impairs the function of some enzymes and cells involved in wound healing. Applying a wound dressing material with an appropriate pH level can help maintain the natural pH balance of the wounded area and reduce CO_2 loss, preventing further damage. Measuring the wound pH level is now a common diagnostic indicator that helps in successful wound management. Therefore, controlling the pH level of the wounded area through dressings is crucial.[82–86] The optimal pH of wound dressing materials is not stable. Regarding the type and stage of the wound and functionality of the dressing material, the optimum pH level can be dynamic and adaptive.[87] Nevertheless, by and large, the slightly acidic pH value has been considered favorable for wound healing. Because human-pathogenic bacteria need pH values above 6 to grow, lower pH values inhibit bacterial growth. Moreover, infected or chronic wounds have a pH above 7.3, while healing wounds have a slightly acidic pH.[88] Besides controlling wound infection, the slightly acidic pH may also change the destructive enzyme activity, release oxygen, promote cell migration, enhancing epithelization and angiogenesis.[82]

As illustrated in **Figure 7**, the solution-immersed pH value of the C-1 control sample (without HPO) was 8.37 (alkaline) after 3 h, decreased to 7.31 at the end of 24 h. On the other hand, solution-immersed pH values of HPO encapsulated nanofiber mats E-2, E-3, and E-4 reached slightly acidic values such as 6.65, 6.62, and 6.94, respectively, which are more convenient for wound healing, at the end of 24 h.

HPO included samples, E-2, E-3, and E-4, showed lower pH levels compared to the oil-free control sample C-1. Since HPO was obtained by an infusion of the *H. Perforatum* plant inside olive oil,[22,23] this decline in pH levels was attributed to the existence of the long-chain free fatty acids such as oleic acid, which was present in olive oil.[73] As shown in Figure 7, it is clear that the inclusion of HPO incorporation resulted in making nanofiber

© 2025 The Author(s). Macromolecular Materials and Engineering published by Wiley-VCH GmbH

14392054, 2025, 10, Downloaded from https://onlinelibrary.wiley.com/doi/10.1002/mame.202500015 by Turkey Cochrane Evidence Aid, Wiley Online Library on [20/10/2026]. See the Terms and Conditions (https://onlinelibrary.wiley.com/terms-and-conditions) on Wiley Online Library for rules of use; OA articles are governed by the applicable Creative Commons License

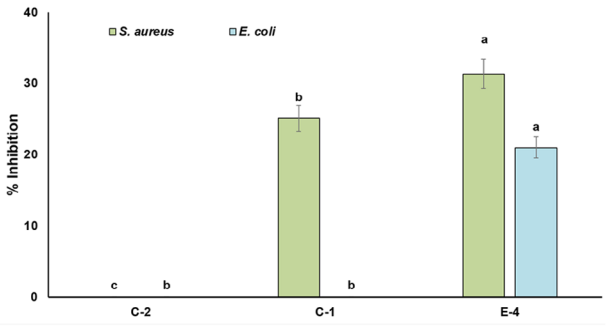


Figure 8. The antibacterial efficiency results performed by OD technique: C-2, C-1, and E-4. Different lowercase letters show significantly different ($p < 0.05$) between microorganism.

mats slightly acidic, which was envisaged to contribute to wound healing in E-2, E-3, and E-4 compared to the HPO-free C-1 control mat. Based on the characterization results, it was decided to continue with the E-4 sample for further studies since there is not any clear difference between the properties of samples having HPO. The sample, having the highest HPO content, E-4, was chosen due to the wound healing and antibacterial properties of HPO.

3.7. Antibacterial Activity Test

The predominant component that will provide antibacterial activity in the obtained TPU nanofiber mats is HPO. The tannic acid used for crosslinking of the gelatin also contributes to this activity.

HPO contains bioactive components like hyperforin and hypericin that have antibacterial properties.[36] The hyperforin component in HPO is effective against Gram-positive bacteria only when present in high concentrations, but it is not always effective against Gram-negative bacteria.[36,89] Additionally, HPO can be effective against resistant bacteria like methicillin-resistant *S. aureus* (MRSA). Aside from its antibacterial activity, *H. perforatum* is known for reducing the duration of inflammation period, fastening epithelialization,[90–92] and promoting efficient wound healing.[36] While numerous studies confirmed the antibacterial activity of HPO,[37,93,94] there are only a few studies in the literature about the incorporation of HPO into a polymer matrix by electrospinning technique.[48,78,79] Further research on this topic is needed.

In this study, the antibacterial activities of TPU nanofiber mats were evaluated by the OD technique for C-1 and C-2 control samples, as well as the 12% HPO-incorporated TPU nanofiber E-4 mat against *E. coli* and *S. aureus*, due to the majority of documented open wound infections are associated with *E. coli* and *S. aureus*. As seen in **Figure 8**, nanofiber mat C-2 did not have an antibacterial activity against *S. aureus* and *E. coli*. On the other hand, the nanofiber C-1 exhibited 25.1 ± 1.8% bacterial inhibition against *S. aureus*. This antimicrobial activity was associated with the tannic acid crosslinker, which is known for its efficiency against Gram-positive bacteria.[94] In the case of the E-4 sample, HPO inclusion improved the antibacterial activity against S. aureus from 25.1 ± 1.8% to 31.3 ± 2.1% which was showed significantly higher antibacterial activity than HPO free C-1 sample ($p < 0.05$). However, there is no significant differences of antibacterial activity between C-2 and C-1 samples against *E. coli*. Moreover, although the C-1 sample could not have any inhibition effect against *E. coli* bacteria, the E-4 sample showed a 21.0 ± 1.5% efficiency. However, it is hard to break down the double membrane structure of Gram-negative bacteria (as in *E. coli*), and the HPO incorporation promoted the antibacterial efficiency of the nanofiber mat. The bioactive constituents of HPO encompass 2,6-dimethyl-heptane (6.25–36.07%), β-pinene (18.32%), α-pinene (5.56–30.92%), δ-cadinene (0.0–22.58%), γ-cadinene (0.0–16.9%), and caryophyllene (15.26%); at this point lower antibacterial efficacy may result from the lower concentration of essential oil in the nanofiber. Similar results were reported by several researchers.[95,96] The bacterial reduction of *E. coli* and *S. aureus* was reported higher than 90% in the composite containing zinc oxide and zinc oxide nanoparticles, in the literature.[97,98] However, lower antibacterial activity of essential oils than metal nanoparticles was reported in the literature. Poly(Caprolactone)/gelatin nanofiber composites incorporated with clove essential oil exhibited a bacterial viability of around 90%, whereas control samples demonstrated 100% viability against *S. aureus*.[99] Similarly, Güneş and Tıhmınlıoğlu (2017)[90] demonstrated that pure chitosan and oil-infused chitosan films had antibacterial efficacy against *S. aureus* and *E. coli*. Nevertheless, at lower concentrations, only a little increasement in antibacterial activity was observed. Similar results were reported by Sasan et al. (2024).[100] Unexpectedly, *Salvia abrotanoides* essential oil (SAEO) addition exhibited little to no antibacterial action maybe attributable to the low dose of SAEO employed in the biodegradable PCL/alginate core-shell nanofibers containing SAEO and ZnO nanoparticles.[98] From this point of view, lower antibacterial activity of essential oil in nanofibers has been observed in different results. Thus, HPO is evaluated as a natural component that makes a difference in wound dressing applications with its antibacterial properties and as a cost-effective medicinal plant extract that supports wound healing.

3.8. In Vitro Wound Healing Test

An in vitro wound healing assay is used to observe how cells close a gap (wound) in a cell monolayer. To test the wound healing properties of the E-4 sample (a TPU nanofiber mat containing 12% HPO), an in vitro scratch wound assay was conducted. The assay demonstrated that the E-4 sample had no negative effect on the fibroblast cells' ability to close the wound. There was no observable difference in the migration or proliferation of the fibroblast cells in the presence of the E-4 sample compared to the control group, suggesting that the sample did not influence the intrinsic wound healing properties of the fibroblast cells and was biocompatible (**Figure 9**).

While the average fiber diameter of the neat electrospun TPU fibers in this study falls within the micrometer range, in line with existing literature, our approach successfully integrated TPU with FSG and HPO to enhance biocompati-

 © 2025 The Author(s). Macromolecular Materials and Engineering published by Wiley-VCH GmbH

14392054, 2025, 10, Downloaded from https://onlinelibrary.wiley.com/doi/10.1002/mame.202500015 by Turkey Cochrane Evidence Aid, Wiley Online Library on [20/10/2026]. See the Terms and Conditions (https://onlinelibrary.wiley.com/terms-and-conditions) on Wiley Online Library for rules of use; OA articles are governed by the applicable Creative Commons License

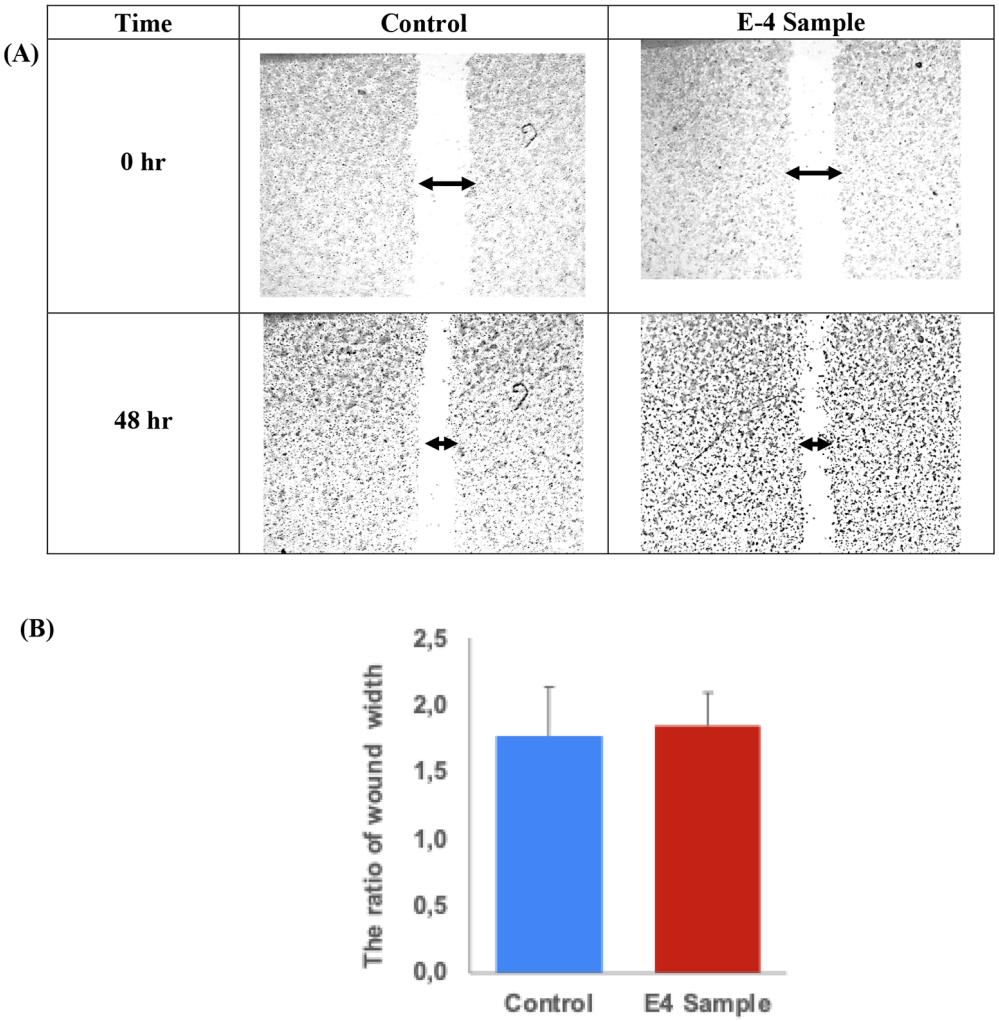


Figure 9. Wound healing assay results. a) Representative microscopic images of cells treated with growth medium only (control) or growth medium containing the E-4 sample (E-4 sample). Images were captured at the beginning of the treatment (0 h) and after 48 h of treatment (48 h). b) The ratio of wound width at 0 h to that at 48 h was calculated ($p \leq 0.05$).

bility, wound healing, and antibacterial properties. Moreover, this combination effectively reduced the fiber diameter to the 250–650 nm range, which has been shown in the literature to promote cell adhesion, growth, proliferation and accelerate wound healing,[52–54] and also achieve close biomimicry of the ECM.[52]

4. Conclusion

In this study, for the first time thermoplastic polyurethane (TPU), FSG, and HPO were combined to form a new type of multifunctional nanofiber material by using the emulsion electrospinning technique. The average diameters of the defect-free TPU nanofiber mats with different concentrations of HPO were ≈250–650 nm, which is suitable for mimicking the native ECM. FTIR analysis showed the interactions between TPU and FSG in the nanofiber mats and confirmed the presence of HPO through the characteristic absorbance peak at 1 741 cm^{-1}. The inclusion of HPO reduced the pH value of the external solution containing the nanofiber mat to slightly acidic levels, which has a positive effect on wound healing. Although there was no antibacterial activity in the control sample C-2, E-4 sample containing HPO demonstrated 31.3% inhibition against *S. auerus* and 21.0% against *E.coli*. Moreover, the E-4 sample was non-toxic to the cells and tended to promote healing in in vitro wound healing assay. Overall, encapsulating the HPO, a natural plant-based, cost-effective bioactive component, in the TPU-gelatin nanofiber mats indicated the potential of fabricated mats as an effective candidate for wound dressing applications.

© 2025 The Author(s). Macromolecular Materials and Engineering published by Wiley-VCH GmbH

14392054, 2025, 10, Downloaded from https://onlinelibrary.wiley.com/doi/10.1002/mame.202500015 by Turkey Cochrane Evidence Aid, Wiley Online Library on [20/10/2026]. See the Terms and Conditions (https://onlinelibrary.wiley.com/terms-and-conditions) on Wiley Online Library for rules of use; OA articles are governed by the applicable Creative Commons License

Appendix

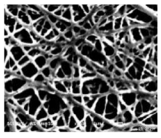
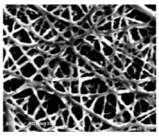
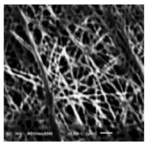
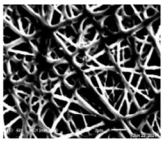
Samples	E-1 (5% HPO)	E-2 (8% HPO)	E-3 (10 %HPO)	E-4 (12 %HPO)
Emulsions				
After Electrospining on Mat				
SEM Images				
Average diameters	410 ± 158 nm	424 ± 157 nm	466 ± 192 nm	514 ± 136 nm

Figure A1. The Preparation HPO Incorporated TPU Nanofiber.

Conflict of Interest

The authors declare no conflict of interest.

Data Availability Statement

The data that support the findings of this study are available from the corresponding author upon reasonable request.

Keywords

emulsion electrospinning, fish skin gelatin (FSG), *H. perforatum* oil, thermoplastic polyurethane, wound dressing

Received: January 12, 2025
Revised: May 8, 2025
Published online: June 4, 2025

[1] S. Jaganathan, M. Mani, A. Khudzari, *Polymers* **2019**, *11*, 586.
[2] P. Mistry, R. Chhabra, S. Muke, A. Narvekar, S. Sathaye, R. Jain, P. Dandekar, *Mater. Sci. Eng., C* **2021**, *119*, 111316.
[3] M. Senevirathne, *Adv. Food Nutr. Res.* **2012**, *65*, 495.
[4] P. Sagitha, C. R. Reshmi, O. Manaf, S. P. Sundaran, J. Kandiyil, S. Athiyanathil, *Nanocomposite Membranes for Water and Gas Separation* **2020**, 199.
[5] H. S. SalehHudin, E. N. Mohamad, W. N. L. Mahadi, A. M Afifi, *Mater. Manuf. Processes* **2018**, *33*, 479.
[6] Yang, Weimin, *Micro and Nano Technologies* **2019**, 339.
[7] X. Qin, *Electrospun Nanofibers* **2017**, 41.
[8] I. Partheniadis, I. Nikolakakis, I. Laidmäe, J. Heinämäki, *Processes* **2020**, *8*, 673.
[9] M. Yu, R. Dong, X. Yan, G. Yu, M. You, X. Ning, Y. Long, *Macromol. Mater. Eng.* **2017**, *302*, 1700002.
[10] H. Zhong, Z. Zhang, M. Wang, Y. Fang, K. Liu, J. Yin, J. Wu, J. Du, *Biomater. Sci.* **2025**, *13*, 697.
[11] H. Zhong, J. Huang, M. Luo, Y. Fang, X. Zeng, J. Wu, J. Du, *Nano Res.* **2023**, *16*, 599.
[12] C. Zhang, F. Feng, H. Zhang, *Trends Food Sci. Technol.* **2018**, *80*, 175.
[13] N. Nikmaram, S. Roohinejad, S. Hashemi, M. Koubaa, F. J. Barba, A. Abbaspourrad, R. Greiner, *RSC Adv.* **2017**, *46*, 28951.
[14] Z. Cui, J. Lin, C. Zhan, J. Wu, S. Shen, J. Si, Q. Wang, *J. Biomater. Sci. Polym. Ed.* **2020**, *31*, 561.
[15] Y. Liu, Q. Li, H. Liu, H. Cheng, J. Yu, Z. Guo, *Chin. J. Polym. Sci.* **2017**, *35*, 713.
[16] S. Habibi, M. Saket, H. Nazockdast, K. Hajinasrollah, *J. Text. Inst.* **2019**, *110*, 1672.
[17] J. Lei, G. Yao, Z. Sun, B. Wang, C. Yu, S. Zheng, *J. Mater. Sci.* **2019**, *54*, 11682.
[18] K. S., P. S. G., K. S. W., K. S. W., J. K., *Macromol. Mater. Eng.* **2016**, *301*, 818.
[19] S. Samimi Gharaie, S. Habibi, H. Nazockdast, *J. Text. Fibrous Mater.* **2018**, *1*.
[20] C. Liu, H. Shi, H. Yang, S. Yan, S. Luan, Y. Li, M. Teng, A. F. Khan, J. Yin, *Mater. Des.* **2017**, *120*, 128.
[21] H. S. Sofi, T. Akram, A. H. Tamboli, A. Majeed, N. Shabir, F. A. Sheikh, *Int. J. Pharm.* **2019**, *569*, 118590.
[22] M. Cui, Z. Chai, Y. Lu, J. Zhu, J. Chen, *Res. Chem. Mater.* **2023**, *2*, 262.
[23] W. Liang, N. Ni, Y. Huang, C. Lin, *Polymers* **2023**, *15*, 4301.
[24] P. Mistry, R. Chhabra, S. Muke, A. Narvekar, S. Sathaye, R. Jain, P. Dandekar, *Mater. Sci. Eng., C* **2021**, *119*, 111316.

 © 2025 The Author(s). Macromolecular Materials and Engineering published by Wiley-VCH GmbH

14392054, 2025, 10, Downloaded from https://onlinelibrary.wiley.com/doi/10.1002/mame.202500015 by Turkey Cochrane Evidence Aid, Wiley Online Library on [20/10/2026]. See the Terms and Conditions (https://onlinelibrary.wiley.com/terms-and-conditions) on Wiley Online Library for rules of use; OA articles are governed by the applicable Creative Commons License

[25] H. Cao, J. Wang, Z. Hao, D. Zhao, *Front. Pharmacol.* **2024**, *15*, 1398939.
[26] A. Rabel, A. H., A. A. M., *MRS Commun.* **2020**, *7*, 416.
[27] L. I. F. Moura, A. M. A. Dias, E. Carvalho, H. C. De Sousa, *Acta Biomater.* **2013**, *9*, 7093.
[28] S. Jana, P. Ghosh, P. Das, S. Nandi, *"Collagen and Gelatin from Fish Processing By-Products for Biomedical Applications"*, (Eds. Maqsood, S., Naseer, M.N., Benjakul, S., Zaidi, A.A.), Springer, Singapore **2024**.
[29] A. A. Karim, R. Bhat, *Food Hydrocolloids* **2009**, *23*, 563.
[30] S. Sreeja, J. Satya, K. Tamilarutselvi, R. Rajajeyasekar, A. Tamilselvi, P. Nandhakumari, K. Sarojini, *Biomass Convers. Biorefin.* **2024**, *14*, 22161.
[31] J. M. Joy, A. Padmaprakashan, A. Pradeep, P. T. Paul, R. J. Mannuthy, S. Mathew, *Foods* **2024**, *13*, 2793.
[32] A. Wierzbicka, M. Bartniak, J. Waśko, B. Kolesińska, J. Grabarczyk, D. Bociaga, *Gels* **2024**, *10*, 491.
[33] S. R. Gomes, G. Rodrigues, G. G. Martins, M. A. Roberto, M. Mafra, C. M. R. Henriques, J. C. Silva, *Mater. Sci. Eng., C* **2015**, *46*, 348.
[34] T. Ren, J. Gan, L. Zhou, H. Chen, *Polymers* **2020**, *12*, 1729.
[35] N. Bölgen, D. Demir, M. S. Yalçın, S. Özdemir, *Int. J. Biol. Macromol.* **2020**, *161*, 1581.
[36] Z. Saddiqe, I. Naeem, A. Maimoona, *J. Ethnopharmacol.* **2010**, *131*, 511.
[37] N. Radulović, V. Stankov-Jovanović, G. Stojanović, A. Šmelcerović, M. Spiteller, Y. Asakawa, *Food Chem.* **2007**, *103*, 15.
[38] P. K. Mukherjee, A. W., "Hypericum Source of Natural Antimicrobials". **2003**.
[39] H. Haidari, S. Garg, K. Vasilev, Z. Kopecki, A. Cowin, *Wound Practice and Research* **2020**, *28*, 173.
[40] K Y. Woo, "Silver Versus Iodine," Advances in Skin and Wound Care.
[41] I. Süntar, E. K. Akkol, H. Keleş, A. Oktem, K. H. C. Başer, E. Yeşilada, *J. Ethnopharmacol.* **2011**, *134*, 89.
[42] M. Abrigo, S. L. McArthur, P. Kingshott, *Macromol. Biosci.* **2014**, *14*, 772.
[43] A. G. Kanani, H. Bahrami, *Trends Biomater. Artif. Organs* **2010**, *24*, 93.
[44] F. Parın, U. Parın, *ChemistrySelect* **2022**, *7*, 202104148.
[45] S. Saghebasl, H. Amini, A. Nobakht, S. Haiaty, H. Bagheri, P. Hasanpour, M. Milani, S. Saghati, O. Naturi, M. Farhadi, R. Rahbarghazi, *J. Nanobiotechnol.* **2023**, *21*, 313.
[46] T. M. Ewedah, A. Abdalla, R. S. Hagag, S. F. Elhabal, K. R. Shoueir, *Int. J. Pharm.* **2024**, *663*, 124541.
[47] Ö. Güner Yılmaz, C. Cam, B. Kocaaga, S. Batirel, S. Guner, *J. Appl. Polym. Sci.* **2018**, *135*.
[48] M. Uzun, A. S., *J. Biomed. Eng. Technol.* **2013**, *1*, 1.
[49] "BS EN 13726-1:2002 Test methods for primary wound dressings. Aspects of absorbency (British Standard)".
[50] A. Akturk, *ACS Omega* **2023**, *8*, 5553.
[51] K. Shanmugam, S. Sundaramoorthy, *RSC Adv.* **2015**, *5*, 31352.
[52] E. CHONG, T. PHAN, I. LIM, Y. ZHANG, B. BAY, S. RAMAKRISHNA, C. LIM, *Acta Biomater.* **2007**, *3*, 321.
[53] A. R. Unnithan, G. Gnanasekaran, Y. Sathishkumar, Y. S. Lee, C. S. Kim, *Carbohydr. Polym.* **2014**, *102*, 884.
[54] Y. Wang, P. Li, P. Xiang, J. Lu, J. Yuan, J. Shen, *J. Mater. Chem. B* **2016**, *4*, 635.
[55] C. Guignot, N. Betz, B. Legendre, A. L. Moel, N. Yagoubi, *Nucl. Instrum. Methods Phys. Res. B* **2001**, *185*, 100.
[56] R. E. Solís-Correa, R. Vargas-Coronado, M. Aguilar-Vega, J. V. Cauich-Rodríguez, J. S. Román, A. Marcos, *J. Biomater. Sci., Polym. Ed.* **2007**, *5*, 561.
[57] S J. McCarthy, G F. Meijs, N. Mitchell, P A. Gunatillake, G. Heath, A. Brandwood, K. Schindhelm, *Biomaterials* **1997**, *18*, 1387.
[58] L. Ponez, F. C. Sentanin, S. R. Majid, A. K. Arof, A. Pawlicka, *Mol. Cryst. Liq. Cryst.* **2012**, *554*, 239.
[59] T. J. Gownolla, M. Raghavendra, *RSC Adv.* **2014**, *4*, 3494.
[60] S. Parvez, M. Rahman, M. Khan, A. Khan, J. Islam, M. Ahmed, M. Rahman, B. Ahmed, *Polym. Bull.* **2012**, *69*, 715.
[61] A. Pakolpakçil, Z. Draczynski, J. Szulc, D. Stawski, N. Tarzynska, A. Bednarowicz, D. Sikorski, C. Hernandez, S. Sztajnowski, I. Krucinska, B. Gutarowska, *Appl. Sci.* **2021**, *11*, 8219.
[62] C. Hacker, Z. Karahaliloglu, G. Seide, E. B. Denkbas, T. Gries, *J. Appl. Polym. Sci.* **2013**, *131*.
[63] N. R. James, J. Philip, A. Jayakrishnan, *Biomaterials* **2006**, *27*, 160.
[64] M. M. Abolfazl Mozaffari, *Indian J. Fibre Text. Res.* **2020**, *45*, 153.
[65] M. Rahman, K. Dey, F. Parvin, N. Sharmin, R A. Khan, B. Sarker, S. Nahar, S. Ghoshal, M. A. Khan, M. M Billah, H U. Zaman, A. M. S. Chowdhury, *Int. J. Polym. Mater. Polym. Biomater.* **2011**, *13*, 1056.
[66] T. H. C. Salles, C. B. Lombello, M. A. d'Ávila, *Mater. Res.* **2015**, *18*, 509.
[67] R. B. Trinca, C. B. Westin, J. A. F. da Silva, Â. M. Moraes, *Eur. Polym. J.* **2017**, *88*, 161.
[68] Ö. Eğri, N. Erdemir, *Artif. Cells Nanomed. Biotechnol.* **2019**, *47*, 1404.
[69] R. Latour, *Encyclopedia of Biomaterials and Biomedical Engineering Second Edition – Four Volume Set* **2008**, 270.
[70] V. Balasubramanian, N. K. Gopi, R. W. Babu, T. V. Thiruvengadam, S. S. M. Subramanian, *J Biomed. Mater. Res.* **1999**, *44*, 253.
[71] C. Zhao, X. Liu, M. Nomizu, N. Nishi, *Biomaterials* **2003**, *24*, 3747.
[72] A. I. M. S. Mohy Eldin, *Int. J. Adv. Res.* **2015**, *3*, 908.
[73] L. Tang, J. W. Eaton, *Am. J. Clin. Pathol.* **1995**, *103*, 466.
[74] H. Adeli, M. T. Khorasani, M. Parvazinia, *Int. J. Biol. Macromol.* **2019**, *122*, 238.
[75] N. Naseri, C. Algan, V. Jacobs, M. John, K. Oksman, A. P. Mathew, *Carbohydr. Polym.* **2014**, *109*, 7.
[76] K. Nuutila, E. Eriksson, *Adv. Wound Care* **2021**, *10*, 685.
[77] P. Wu, E. A. Nelson, W. H. Reid, C. V. Ruckley, J. D. S. Gaylor, *Biomaterials* **1996**, *17*, 1373.
[78] A. Nurzynska, K. Klimek, K. Palka, Ł. Szajnecki, G. Ginalska, *Materials* **2021**, *14*, 2344.
[79] S. Y. Gu, Z. M. Wang, J. Ren, C. Y. Zhang, *Mater. Sci. Eng., C* **2009**, *29*, 1822.
[80] C. L. Zehrer, D. Holm, S. E. Solfest, S. Walters, *Int. Wound J.* **2013**, *11*, 681.
[81] P. Beldon, *Wounds UK* **2008**, *4*, 74.
[82] E. Conde, "The interest of pH in wound healing," Retrieved: **2021**.
[83] B. Greener, A. Hughes, N. Bannister, J. Douglass, *J. Wound Care* **2005**, *14*, 59.
[84] S. D. Connolly, *"The influence of different dressings on the pH of the wound environment"*, University of Strathclyde, Biomedical Engineering, Glasgow, Scotland, UK **2022**.
[85] E. M. Jones, C. A. Cochrane, S. L. Percival, *Adv. Wound Care* **2015**, *4*, 431.
[86] L. Bennison, C. Miller, R. Summers, A. Minnis, G. Sussman, W. McGuiness, *Wounds Australia Journal (Wound Practice and Research)* **2017**, *25*, 63.
[87] Z. Han, M. Yuan, L. Liu, K. Zhang, B. Zhao, B. He, Y. Liang, F. Li, *Nanoscale Horiz.* **2023**, *8*, 422.
[88] L. A. Schneider, A. Korber, S. Grabbe, J. Dissemond, *Arch. Dermatol. Res.* **2006**, *298*, 413.
[89] A. Pulok, K. Mukherjee, *Orient Pharm Exp Med* **2003**, *3*, 11.
[90] S. Gunes, S. Tamburaci, F. Tihminlioglu, *J. Mater. Sci.: Mater. Med.* **2020**, *31*, 7.
[91] I. P. Süntar, E. K. Akkol, D. Yilmazer, T. Baykal, H. Kirmizibekmez, M. Alper, E. Yeşilada, *J. Ethnopharmacol.* **2010**, *127*, 468.
[92] S. Kıyan, Y. Uzun, *Turkish J. Trauma Emerg. Surg.* **2015**, *21*, 323.
[93] F. Pourhojat, M. Sohrabi, S. Shariati, H. Mahdavi, L. Asadpour, *Res. Chem. Intermed.* **2017**, *43*, 297.

 © 2025 The Author(s). Macromolecular Materials and Engineering published by Wiley-VCH GmbH

14392054, 2025, 10, Downloaded from https://onlinelibrary.wiley.com/doi/10.1002/mame.202500015 by Turkey Cochrane Evidence Aid, Wiley Online Library on [20/10/2026]. See the Terms and Conditions (https://onlinelibrary.wiley.com/terms-and-conditions) on Wiley Online Library for rules of use; OA articles are governed by the applicable Creative Commons License

[94] K. T., S. J., Y. Jung, *Elsevier Food Chemistry* **2011**, 116.
[95] K. Kachare, S. Shendage, S. Matwal, M. Walvekar, S. Vhanbatte, J. Chang, A. Ghule, *Surf. Coat. Technol.* **2024**, *491*, 131171.
[96] K. Lefatshe, C M. Muiva, L P. Kebaabetswe, *Carbohydr. Polym.* **2017**, *164*, 301.
[97] R. Ahmed, M. Tariq, I. Ali, R. Asghar, P. Noorunnisa Khanam, R. Augustine, A. Hasan, *Int. J. Biol. Macromol.* **2018**, *120*, 385.
[98] H. Liu, Y. Yang, L. Deng, Z. Shen, Q. Huang, N. G. Shah, W. Chen, Y. Zhang, X. Wang, L. Yu, Z. Chen, *Int. J. Biol. Macromol.* **2024**, *279*, 135177.
[99] T. Kim, J. Silva, Y. Jung, *Food Chem.* **2011**, *126*, 116.
[100] S. Sasan, A. M. Molavi, K. H. Moqadam, N. Farrokhi, F. Oroojalian, *Int. J. Biol. Macromol.* **2024**, *279*, 135152.

 © 2025 The Author(s). Macromolecular Materials and Engineering published by Wiley-VCH GmbH

14392054, 2025, 10, Downloaded from https://onlinelibrary.wiley.com/doi/10.1002/mame.202500015 by Turkey Cochrane Evidence Aid, Wiley Online Library on [20/10/2026]. See the Terms and Conditions (https://onlinelibrary.wiley.com/terms-and-conditions) on Wiley Online Library for rules of use; OA articles are governed by the applicable Creative Commons License